

MLAAN: Scaling Supervised Local Learning with Multilaminar Leap Augmented Auxiliary Network

Yuming Zhang*, Shouxin Zhang*, Peizhe Wang*, Feiyu Zhu, Dongzhi Guan†, Junhao Su, Jiabin Liu, Changpeng Cai†

Abstract

Deep neural networks (DNNs) typically employ an end-to-end (E2E) training paradigm which presents several challenges, including high GPU memory consumption, inefficiency, and difficulties in model parallelization during training. Recent research has sought to address these issues, with one promising approach being local learning. This method involves partitioning the backbone network into gradient-isolated modules and manually designing auxiliary networks to train these local modules. Existing methods often neglect the interaction of information between local modules, leading to myopic issues and a performance gap compared to E2E training. To address these limitations, we propose the Multilaminar Leap Augmented Auxiliary Network (MLAAN). Specifically, MLAAN comprises Multilaminar Local Modules (MLM) and Leap Augmented Modules (LAM). MLM captures both local and global features through independent and cascaded auxiliary networks, alleviating performance issues caused by insufficient global features. However, overly simplistic auxiliary networks can impede MLM’s ability to capture global information. To address this, we further design LAM, an enhanced auxiliary network that uses the Exponential Moving Average (EMA) method to facilitate information exchange between local modules, thereby mitigating the shortsightedness resulting from inadequate interaction. The synergy between MLM and LAM has demonstrated excellent performance. Our experiments on the CIFAR-10, STL-10, SVHN, and ImageNet datasets show that MLAAN can be seamlessly integrated into existing local learning frameworks, significantly enhancing their performance and even surpassing end-to-end (E2E) training methods, while also reducing GPU memory consumption.

Introduction

End-to-end (E2E) backpropagation, a mainstream method for training deep neural networks, has achieved remarkable success in image segmentation (Wang, Peng, and Liu 2018), target tracking (Bao et al. 2022), visual sound separation (He et al. 2021), and other fields. Despite these accomplishments, E2E learning has its drawbacks. It necessitates retaining the complete computational graph and all intermediate activations post each local module’s computation (Wang et al. 2021a), increasing GPU memory usage. As network depth and model complexity grow, this memory demand can severely constrain the training on high-resolution data inputs

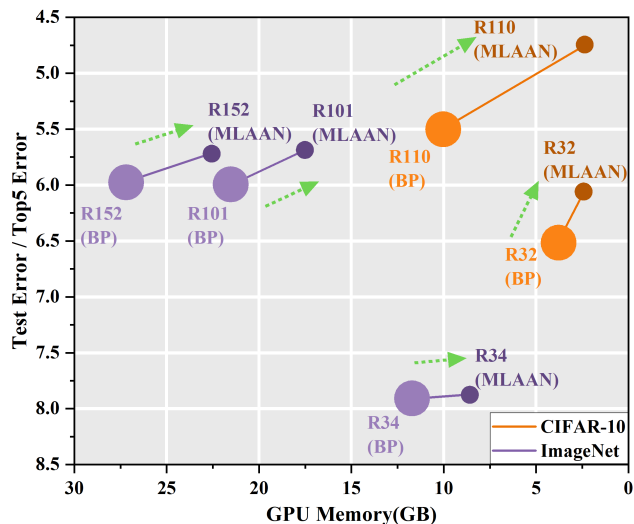


Figure 1: Comparison between different methods with MLAAN and BP regarding GPU Memory, Test Error, and Top5 Error. Results are obtained using ResNet-32 and ResNet-110 on CIFAR-10, ResNet-34, ResNet-101, and ResNet-152 on ImageNet.

(Wu et al. 2021). Additionally, the E2E structure delays parameter updates in initial layers until the entire forward and backward propagation cycles conclude, causing inefficiency (Jaderberg et al. 2017a), (Salimans et al. 2017). This sequential gradient processing also impedes model parallelization (Löwe, O’Connor, and Veeling 2019a), (Belilovsky, Eickenberg, and Oyallon 2020) and raises biological plausibility concerns due to its reliance on cross-layer backpropagation (Crick 1989), (Shen, Zhao, and Zeng 2022).

Due to the inherent flaws of E2E training (Illing et al. 2021a), (Xiong, Ren, and Urtasun 2020a), some researchers are exploring local learning as an alternative. Local learning divides the network into gradient-isolated local modules and designs auxiliary networks to assist their training (Bengio et al. 2006). This method eliminates the need for sharing gradients and activation parameters between modules, reducing GPU memory requirements (Wang et al. 2021a). In addition, local learning uses local error signals, which align

more closely with biological feasibility principles. However, the existing focus on local features and the lack of information exchange between local modules significantly lower overall performance than that of E2E training (Mostafa, Ramesh, and Cauwenberghs 2018). Despite some recent improvements in the performance of local learning (Belilovsky, Eickenberg, and Oyallon 2020), (Nøkland and Eidnes 2019), current methods still have myopia issues and insufficient global feature representation, limiting their application in precision-critical tasks. Therefore, the crucial goal of local learning is to ensure that each local module receives ample global information and facilitates information exchange between modules. Maintaining GPU memory efficiency while improving global performance is essential for making local learning a viable alternative to E2E training.

In this paper, we propose the Multilaminar Leap Augmented Auxiliary Network (MLAAN), a novel supervised local learning method, as illustrated in Figure 2. MLAAN employs a dual architecture where the Multilaminar Local Modules (MLM) design divides the network into independent and cascaded levels. The independent level uses standalone auxiliary networks to capture local features, while the cascaded level utilizes cascade auxiliary networks to gain global features through module inter-sharing. The two levels complement each other and sufficiently learn global and local features. Furthermore, we observe that even with multiple local modules sharing weights, the backbone network can still be misled by overly simplistic auxiliary networks, leading to shortsightedness. To resolve this issue, we further design the Leap Augmented Modules (LAM). LAM tackles the problem of weakened supervision caused by overly simplistic auxiliary networks. This module utilizes the network structure of subsequent layers and updates using the Exponential Moving Average (EMA). LAM is strategically placed between the primary and secondary networks within each gradient-isolated module to mitigate myopia. The synergy between MLM and LAM significantly enhances network performance. The efficacy of MLAAN is validated on a suite of benchmark image classification datasets, including CIFAR-10 (Krizhevsky, Hinton et al. 2009), STL-10 (Coates, Ng, and Lee 2011), SVHN (Netzer et al. 2011), and ImageNet (Deng et al. 2009). Experimental results demonstrate that MLAAN almost perfectly resolves the existing issues in local learning.

- We propose a novel framework, MLAAN, which effectively overcomes the traditional limitations of local learning, particularly the challenge of accessing adequate global information and the myopic perspective resulting from limited information exchange.
- MLAAN is a versatile plug-and-play module that can be seamlessly integrated into existing supervised local learning methods, significantly enhancing their performance.
- MLAAN’s effectiveness has been validated on widely used datasets, including CIFAR-10, STL-10, SVHN, and ImageNet, achieving state-of-the-art (SOTA) performance. Remarkably, it surpasses the performance of E2E training while also substantially saving GPU memory.

Related Works

Alternatives of Backpropagation

Traditional E2E learning faces challenges like high GPU memory consumption, reduced training efficiency, difficulties in model parallelization, and poor biological plausibility. Researchers are developing alternative strategies, such as target propagation (Bartunov et al. 2018; Le Cun 1986; Lee et al. 2015), feedback alignment (Lillicrap et al. 2014; Nøkland 2016), synthetic gradients (Jaderberg et al. 2017b), feature replay (Huo, Gu, and Huang 2018), and decoupled parallel backpropagation (Huo et al. 2018), to tackle memory and efficiency issues. Some suggest using forward gradient learning instead of backpropagation (Dellafrera and Kreiman 2022). However, most of these methods still rely on global loss values and have not effectively addressed challenges with large-scale datasets like ImageNet (Deng et al. 2009).

Local Learning

Local learning is considered a promising alternative to traditional E2E methods (Nøkland and Eidnes 2019). However, the lack of local inter-module interaction and poor global performance has hindered its development (Bengio et al. 2006). To improve global performance, some scholars have used self-supervised loss to preserve features during local module propagation (Illing et al. 2021b). For example, Y. Xiong et al. (Xiong, Ren, and Urtasun 2020b) designed SimCLR loss for Local Contrastive Learning. Sindy et al. (Löwe, O’Connor, and Veeling 2019b) applied Comparative Predictive Coding loss to reduce feature loss in Greedy InfoMax. These methods perform well with a few network blocks but struggle with many blocks. Adrien et al.’s method (Journé et al. 2022), combining Hebbian learning with local learning, addresses this issue but faces challenges on large datasets like ImageNet (Deng et al. 2009). Methods like InfoPro (Wang et al. 2021a) and DGL (Belilovsky, Eickenberg, and Oyallon 2020) have improved local learning performance on large datasets such as ImageNet (Deng et al. 2009). However, due to gradient isolation, their performance still falls short of E2E methods. Enhancing inter-module communication to match or surpass E2E performance remains a critical issue.

Based on existing research and shortcomings, this paper aims to design a new method to improve inter-module communication and address model myopia, ultimately enhancing supervised local learning performance and enabling advanced training of large models on resource-limited platforms.

Method

Preparations

To begin, we present an overview of the conventional E2E BP-supervised learning paradigm and the BP mechanism for contextual clarity. Let x and y denote a data sample and its corresponding true label, respectively. The neural network with parameters θ is represented as f_θ , with its forward computation denoted as $f(\cdot)$. In BP, we evaluate the loss function

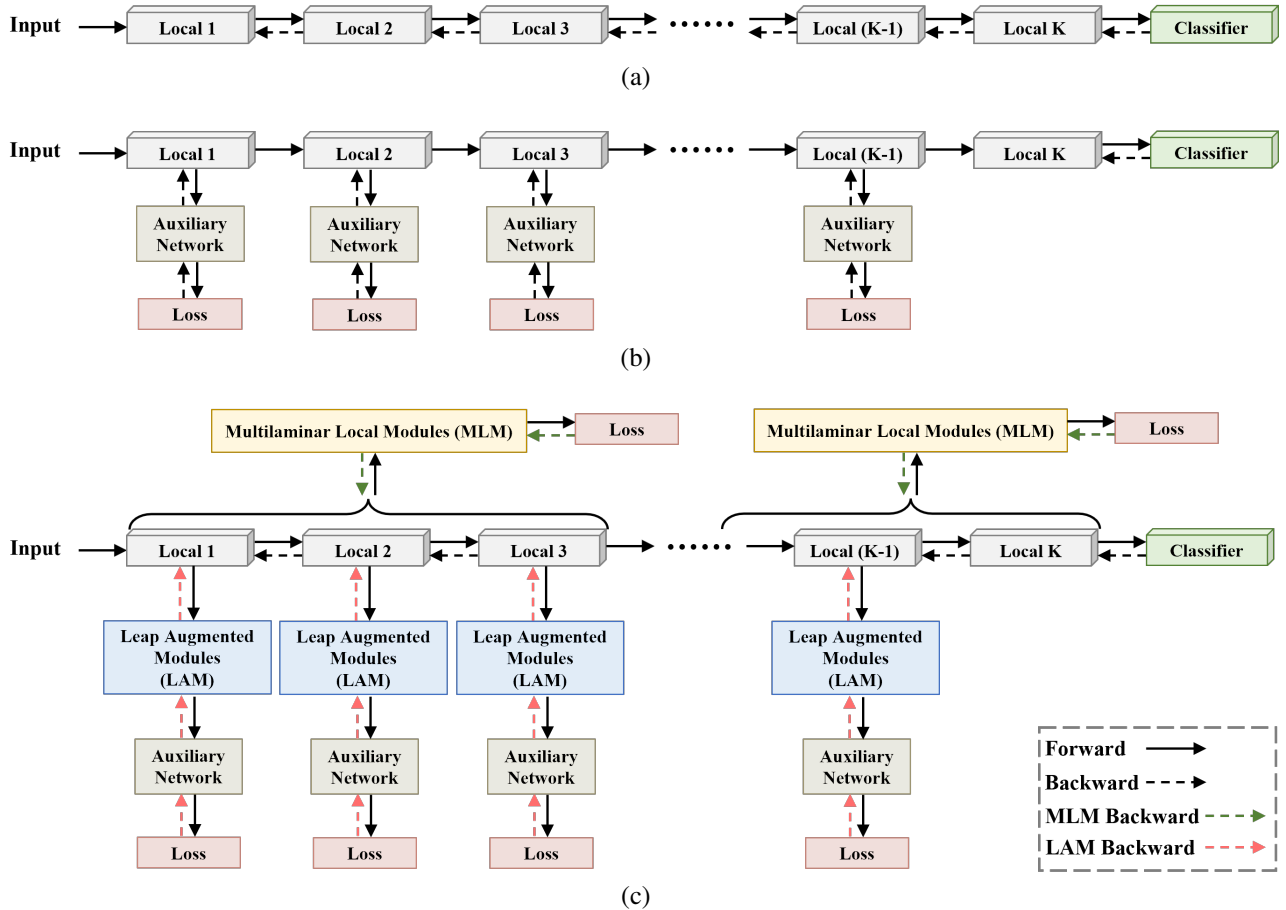


Figure 2: Comparison of (a) E2E backpropagation, (b) other supervised local learning methods, and (c) our proposed method. The details of our method are in Figure 3.

$\mathcal{L}(\hat{y}, y)$ between the output of the last module and the ground truth label, and propagate it back iteratively to the preceding blocks.

Supervised local learning divided the network into multiple local modules, the output of the j -th local module is used as the input of the subsequent $(j + 1)$ -th local module. During forward propagation, $x_{j+1} = f_{\theta_j}(x_j)$. For existing supervised local learning methods, the output of a local module is directed to its auxiliary network to generate local monitoring signals $\hat{y}_j = g_{\gamma_j}(f_{\theta_j}(x_j))$, where $g_{\gamma_j}(\cdot)$ represents the auxiliary network updating function. The updates are made based on the following equations:

$$\gamma_j \leftarrow \gamma_j - \eta_\alpha \times \nabla_{\gamma_j} \mathcal{L}(\hat{y}_j, y) \quad (1)$$

$$\theta_j \leftarrow \theta_j - \eta_\ell \times \nabla_{\theta_j} \mathcal{L}(\hat{y}_j, y) \quad (2)$$

where γ_j, θ_j means updated parameters of the auxiliary networks and the local modules, η_α and η_ℓ denote the learning rate of them.

Multilaminar Local Modules

Current supervised local learning methods face certain limitations in that they rely on auxiliary networks to in-

dependently update each gradient-isolated local module, which restricts the local modules from acquiring global features. Therefore, we propose Multilaminar Local Modules (MLM), designed to facilitate local modules in capturing global features while retaining local features as much as possible.

In our MLM, we divide the entire network into two levels of local modules: cascaded modules and independent modules. Each local module functions independently, while multiple adjacent local modules form a cascaded module.

We assume that each cascaded module computes $K(K > 1)$ consecutive local modules. For the j -th local module within a cascade module, denoted as f_{θ_j} , it receives signals from its independent auxiliary network g_{γ_j} and k cascaded auxiliary networks, $h_{\beta_1}, \dots, h_{\beta_{i+k-1}}$. The local supervision of a particular local module occurs $(K + 1)$ times, once from the loss function of independent modules, $\mathcal{L}(\hat{y}_j, y)$, and k times from loss function of cascaded modules, $\mathcal{L}(\hat{y}_i, y), \dots, \mathcal{L}(\hat{y}_{i+k-1}, y)$.

The updated rules can be summarized as follows:

$$\gamma_j \leftarrow \gamma_j - \eta_\alpha \times \nabla_{\gamma_j} \mathcal{L}(\hat{y}_j, y) \quad (3)$$

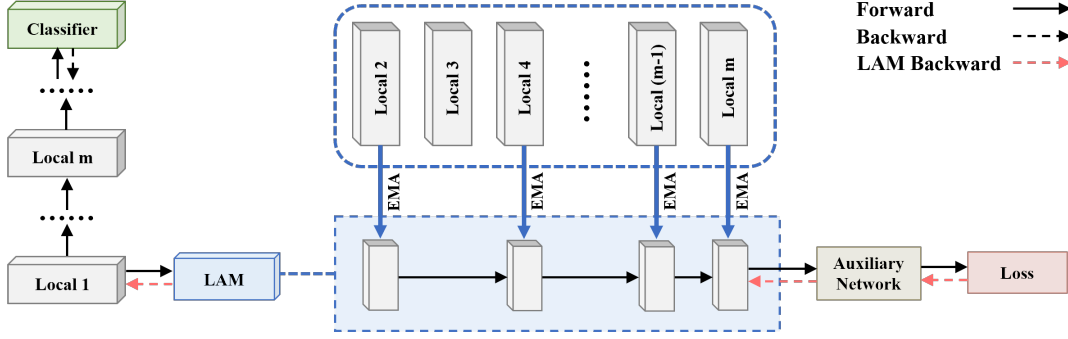


Figure 3: The Leap Augmented Modules architecture. As the proximity to the early blocks increases, the utilization of auxiliary layers employing EMA decreases.

$$\beta_j \leftarrow \beta_j - \sum_{n=i}^{i+k-1} (\eta_c \times \nabla_{\beta_j} \mathcal{L}(\hat{y}_n, y)) \quad (4)$$

$$\theta_j \leftarrow \theta_j - \eta_l \times \nabla_{\theta_j} \mathcal{L}(\hat{y}_j, y) \quad (5)$$

where θ_j means updated parameters of the local modules, γ_j , β_j denote updated parameters of the independent and cascaded auxiliary networks, η_l , η_α , and η_c are the learning rates of them, respectively.

Leap Augmented Modules

After applying MLM, we observe that even when multiple local modules share weights, the backbone network can still be misled by overly simplistic auxiliary networks, leading to insufficient supervision of the hidden layers by local modules and suboptimal learning outcomes. To handle this concern, we introduce generic Leap Augmented Modules (LAM). LAM is designed to enhance the exchange of information between the current local module and subsequent local modules, thereby promoting improved learning outcomes.

As shown in Figure 3, for the j -th local module f_{θ_j} , its auxiliary network is denoted as g_{γ_j} . We assume that f_{θ_j} is expected to receive information from p ($p \geq 1$) hidden layers, distributed across the early, intermediate, and deeper layers of the subsequent local modules. To illustrate how our method is implemented, we assume $p = 1$, meaning that the auxiliary network selects only one hidden layer from subsequent local modules to serve as the enhanced auxiliary network. We perform a deepcopy operation: $\gamma_j^1 = \text{deepcopy}(\theta^{j+i})$ ($i \geq 1$), where θ^{j+i} represents the hidden layer extracted in the $(j+i)$ -th local module. The γ_j^1 receives the information from the hidden layer of the $(j+i)$ -th local modules and is updated using Exponential Moving Average (EMA). The updated rules are as follows:

$$\gamma_j^1 \leftarrow \gamma_j^1 - \eta_\alpha \times \nabla_{\gamma_j^1} \mathcal{L}(\hat{y}_j, y) \quad (6)$$

$$\gamma_j^1 \leftarrow \text{EMA}(\gamma_j^1, \theta_{j+i}) \quad (7)$$

$$\theta_j \leftarrow \theta_j - \eta_l \times \nabla_{\theta_j} \mathcal{L}(\hat{y}_j, y) \quad (8)$$

where γ_j^1 represents the parameters of the first layer of the j -th auxiliary network and θ_j represents those of the j -th local

module, η_α and η_l are the learning rates of them. After updating with local gradients, γ_j^1 undergoes further refinement by incorporating the parameters of the $(j+i)$ -th local module θ_{j+i} via the EMA, which is a weighted sum operation.

Moreover, when $p = 2$, deeper integration is employed by performing a deepcopy operation: $\gamma_j^2 = \text{deepcopy}(\theta^{j+i+k})$ ($i, k \geq 1$), this operation utilizes the information from the $(i+j+k)$ -th local module, allowing for even more robust incorporation of global information into the auxiliary network. When p is larger, the construction of the auxiliary network follows this pattern accordingly. And the j -th auxiliary network will be represented as $\gamma_j = \{\gamma_j^1, \gamma_j^2, \dots\}$ finally.

Multilaminar Leap Augmented Auxiliary Network

MLM and LAM each possess distinct characteristics. MLM captures both local and global features through independent and cascaded auxiliary networks. LAM is further designed to accurately capture local features while avoiding misleading the main network caused by overly simplistic auxiliary networks. Based on their characteristics, we fuse the two approaches to make it a Multilaminar Leap Augmented Auxiliary Network (MLAAN). MLAAN performs exceptionally well under the synergy between MLM and LAM.

One local module, denoted as f_{θ_s} , within its cascaded module, $h_{\beta_s} = \{h_{\beta_s}, h_{\beta_{s+1}}, \dots, h_{\beta_{s+k-1}}\}$. With the application of MLM, f_{θ_s} receives $(K+1)$ local supervisions. Upon incorporating the LAM, the parameters of p hidden layers extracted in corresponding local modules, $\theta_{s+p} = \{\theta_{s+1}, \theta_{s+2}, \dots, \theta_{s+p}\}$, are integrated into the s -th auxiliary network, $\gamma_s = \{\gamma_s^1, \gamma_s^2, \dots, \gamma_s^p\}$. MLM and LAM work in parallel to maximize the utilization of global and local features.

The overall updated rules of MLAAN are described as follows:

$$\gamma_s \leftarrow \gamma_s - \eta_\alpha \times \nabla_{\gamma_s} \mathcal{L}(\hat{y}_j, y) \quad (9)$$

$$\gamma_s \leftarrow \text{EMA}(\gamma_s, \theta_{s+M}) \quad (10)$$

$$\beta_s \leftarrow \beta_s - \sum_{n=i}^{i+k-1} (\eta_c \times \nabla_{\beta_s} \mathcal{L}(\hat{y}_n, y)) \quad (11)$$

$$\theta_s \leftarrow \theta_s - \eta_l \times \nabla_{\theta_s} \mathcal{L}(\hat{y}_s, y) \quad (12)$$

Dataset	Method	ResNet-32		ResNet-110	
		K=8(Test Error)	K=16(Test Error)	K=32(Test Error)	K=55(Test Error)
CIFAR-10	DGL	11.63	14.08	12.51	14.45
	DGL*	6.25±0.12(↓5.26-5.50)	6.36±0.15(↓7.57-7.87)	5.38±0.27(↓6.86-7.40)	5.42±0.52(↓8.51-9.03)
	InfoPro	11.51	12.93	12.26	13.22
	InfoPro*	6.37±0.50(↓4.64-5.14)	6.37±0.35(↓6.21-6.91)	5.41±0.49(↓6.36-7.34)	5.60±0.55(↓7.07-7.62)
	MLAAN	6.36±0.23	6.51±0.55	5.41±0.62	6.02±0.67
BP(ResNet-32)=6.37, BP(ResNet-110)=5.42					
STL-10	DGL	25.05	27.14	25.67	28.16
	DGL*	19.35±0.51(↓5.19-6.21)	19.02±0.11(↓8.01-8.23)	19.54±0.34(↓5.79-6.47)	19.66±0.55(↓7.95-8.50)
	InfoPro	27.32	29.28	28.58	29.20
	InfoPro*	19.21±0.19(↓7.92-8.30)	19.21±0.12(↓9.95-10.19)	19.51±0.16(↓8.91-9.23)	19.24±0.21(↓9.75-10.17)
	MLAAN	19.34±0.15	19.96±0.53	20.46±0.64	19.66±0.67
BP(ResNet-32)=19.35, BP(ResNet-110)=19.67					
SVHN	DGL	4.83	5.05	5.12	5.36
	DGL*	2.79±0.12(↓1.92-2.16)	2.73±0.19(↓2.13-2.51)	2.78±0.22(↓2.12-2.56)	2.90±0.14(↓2.32-2.46)
	InfoPro	5.61	5.97	5.89	6.11
	InfoPro*	2.97±0.18(↓2.46-2.82)	2.95±0.2(↓2.82-3.02)	2.87±0.32(↓2.70-3.34)	2.90±0.42(↓2.79-3.21)
	MLAAN	2.85±0.22	2.82±0.38	2.79±0.31	2.89±0.31
BP(ResNet-32)=2.99, BP(ResNet-110)=2.92					

Table 1: Comparison of supervised local learning methods and BP on image classification datasets. The averaged test errors are reported from three independent trials. The * means the addition of our MLAAN.

where θ_s means the parameters of the s -th local module, γ_s and β_s denote the parameters of its independent and cascaded auxiliary networks, η_l , η_α , and η_c are the learning rates of them, respectively.

Experiments

Experimental Setup

We conduct experiments with ResNet (He et al. 2016) architectures of various depths on CIFAR-10 (Krizhevsky, Hinton et al. 2009), SVHN (Netzer et al. 2011), STL-10 (Coates, Ng, and Lee 2011), and ImageNet (Deng et al. 2009). MLAAN is integrated with DGL (Belilovsky, Eickenberg, and Oyallon 2019) and InfoPro (Wang et al. 2021b) to assess performance and compare with BP (Rumelhart et al. 1985) and original supervised local learning methods. Performance is compared under consistent K conditions, typically $K = 3$, ensuring rigorous and fair evaluation.

Comparison with the SOTA results

Results on Image Classification Benchmarks. We evaluate MLAAN’s performance on CIFAR-10 (Krizhevsky, Hinton et al. 2009), SVHN (Netzer et al. 2011), and STL-10 (Coates, Ng, and Lee 2011) datasets, with results in Table 1.

On CIFAR-10 (Krizhevsky, Hinton et al. 2009), increasing local modules enhances MLAAN’s benefits. For ResNet-32 ($k=16$) (He et al. 2016), the Test Error decreases from 14.08 and 12.93 to 6.36 and 6.37, marking a 55% and 51% improvement over the BP (Rumelhart et al. 1985) baseline. For ResNet-110 ($k=55$) (He et al. 2016), MLAAN with

DGL (Belilovsky, Eickenberg, and Oyallon 2019) and InfoPro (Wang et al. 2021b) improves performance by 61% and 56%, respectively. On STL-10 (Coates, Ng, and Lee 2011), MLAAN achieves over 30% and 34% improvements under the same situations, while on SVHN (Netzer et al. 2011), gains exceed 42% and 49%.

Subsequently, we assess MLAAN on ImageNet (Deng et al. 2009) using ResNet-34 (He et al. 2016) with 17 local modules. Incorporating MLAAN significantly improves performance, as shown in Table 2, reducing both Top1 and Top5 Error by 0.3%, comparable to the BP (Rumelhart et al. 1985) baseline. Further experiments’ performance is also over BP (Rumelhart et al. 1985). ResNet-101 (He et al. 2016) sees Top1 and Top5 Error reductions of 0.09% and 0.7%, while ResNet-152 (He et al. 2016) shows decreases of 0.2% and 0.5%.

Backbone	Method	Top1 Error	Top5 Error
ResNet-34 (K=17)	BP	25.38	7.90
	MLAAN	25.31(↓0.07)	7.88(↓0.02)
ResNet-101 (K=34)	BP	22.03	5.93
	MLAAN	21.69(↓0.34)	5.72(↓0.21)
ResNet-152 (K=51)	BP	21.60	5.92
	MLAAN	21.34(↓0.26)	5.74(↓0.18)

Table 2: Results on the validation set of ImageNet

These results demonstrate MLAAN’s ability to improve deep learning models, bridge performance gaps, and outper-

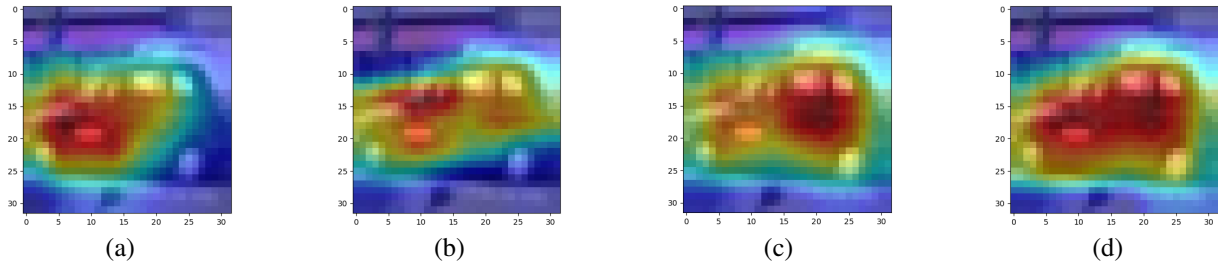


Figure 4: Visualization of feature maps. (a) Feature map of DGL. (b) Feature map of DGL with LAM. (c) Feature map of DGL with MLM. (d) Feature map of DGL with MLAAN.

form BP even with more local modules, reinforcing its effectiveness in improving accuracy and robustness in complex and deep architectures.

Memory Consumption. We investigate the GPU memory usage of BP (Rumelhart et al. 1985) and MLAAN on CIFAR-10 (Krizhevsky, Hinton et al. 2009) and ImageNet (Deng et al. 2009), with results in Table 3.

For ResNet-32 ($k=16$) (He et al. 2016), usage decreases by 22.3% compared to BP (Rumelhart et al. 1985). For ResNet-110 ($k=55$) (He et al. 2016), the reduction is 70.2%. ResNet-34, ResNet-101, and ResNet-152 (He et al. 2016) also show reductions of 15.4%, 1.7%, and 12.5%, respectively, compared to BP (Rumelhart et al. 1985). These findings demonstrate that MLAAN performs better with less GPU memory usage than BP (Rumelhart et al. 1985).

Dataset	Network	Method	GPU Memory(GB)
CIFAR-10	ResNet-32 (K=16)	BP	3.37G
		MLAAN	2.62G(↓22.3%)
	ResNet-110 (K=55)	BP	9.26G
		MLAAN	2.76G(↓70.2%)
ImageNet	ResNet-34 (K=17)	BP	10.74G
		MLAAN	9.09G(↓15.4%)
	ResNet-101 (K=34)	BP	20.64G
		MLAAN	17.93G(↓13.1%)
	ResNet-152 (K=51)	BP	26.29G
	MLAAN	23.01G(↓12.5%)	

Table 3: Comparison of GPU memory usage between BP and MLAAN on CIFAR-10 and ImageNet.

Ablation Study

Comparison of Different Module Combinations. We conduct experiments with ResNet-32 ($K=16$) (He et al. 2016) as the backbone, using DGL (Belilovsky, Eickenberg, and Oyallon 2019) as the baseline, to evaluate MLM, LAM, and MLAAN. The results are summarized in Table 4.

Without MLM and LAM, the Test Error is 14.08. Incorporating MLM individually reduces the Test Error by 5.62 and 6.44, respectively. Combining both modules results in a further reduction to 6.80, a substantial decrease of 7.28. These findings highlight the significant contributions of MLM and

LAM, demonstrating MLAAN’s remarkable performance through their integration.

MLM	LAM	Test Error
×	×	14.08
✓	×	8.46(↓5.62)
×	✓	7.64(↓6.44)
✓	✓	6.36(↓7.28)

Table 4: Ablation study of our method on CIFAR-10.

Comparative Analysis of Unfair Epochs. Undeniably, the utilization of MLAAN introduces additional Wall Time, prompting us to conduct a comparative analysis of unfair epochs. The findings of this analysis can be observed in Table 5. When using DGL (Belilovsky, Eickenberg, and Oyallon 2019) as the baseline, after incorporating MLAAN, it only takes 300 epochs to reduce the Test Error by 45% for a Backbone of ResNet-32 ($K=16$) (He et al. 2016) and 52% for ResNet-110 ($K=55$) (He et al. 2016).

Dataset	Method	ResNet-32 (K=16)	ResNet-110 (K=55)
CIFAR-10	DGL(Epochs=400)	14.08	14.45
	DGL*(Epochs=300)	7.79(↓6.29)	6.98(↓7.47)

Table 5: Comparison of Test Error with different epochs on the CIFAR-10. The * means the addition of MLAAN.

Comparison of Features in Different Methods. To showcase the advanced capabilities of MLAAN, we conduct feature map analyses on different configurations, including DGL (Belilovsky, Eickenberg, and Oyallon 2019), DGL with MLM, DGL with LAM, and DGL with MLAAN. The resulting figures detailing these feature maps can be found in Figure 4.

Upon analyzing them, we can observe that (a) is concentrated in specific regions, indicating the presence of significant information within those areas. Conversely, after the fusion of (b) and (c), (d) captures more comprehensive global features, including localized edge features. It follows

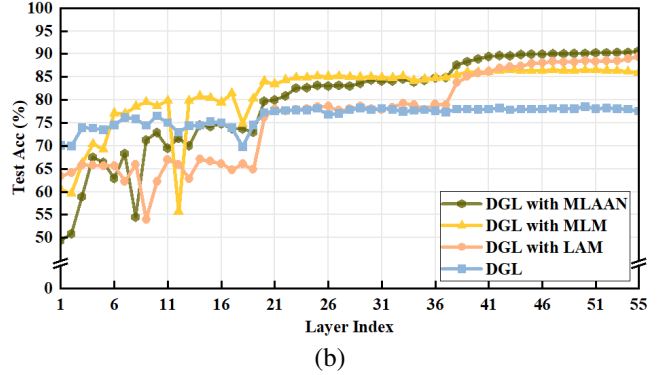
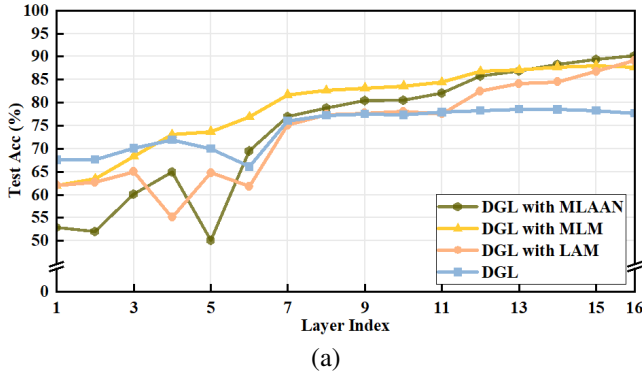


Figure 5: Comparison of layer-wise linear separability. (a) Linear Separability of RestNet-32 on CIFAR-10. (b) Linear Separability of RestNet-110 on CIFAR-10.

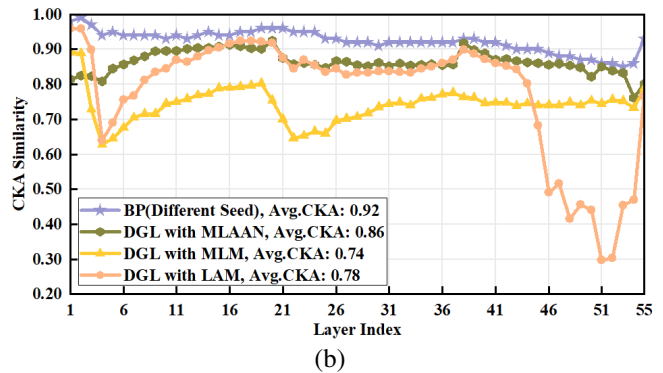
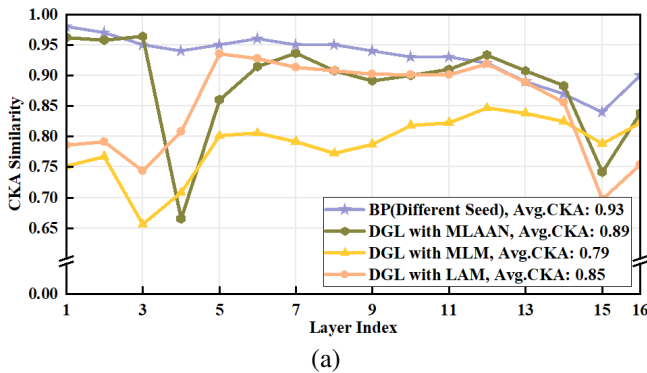


Figure 6: Comparison of layer-wise representation similarity. (a) Representation Similarity of RestNet-32 on CIFAR-10. (b) Representation Similarity of RestNet-110 on CIFAR-10.

that MLAAN can compensate for the shortcomings of other methods.

Decoupled Layer Accuracy Analysis. We have demonstrated that MLAAN achieves accuracy comparable to BP (Rumelhart et al. 1985) across different architectures. To further analyze MLAAN’s impact, we freeze the main network parameters and train a linear classifier for each gradient-isolated layer. Results are shown in Figure 5 using DGL (Belilovsky, Eickenberg, and Oyallon 2019) as the baseline.

High classification accuracy in early layers can hinder global network performance by optimizing local objectives at the expense of features needed by later layers. MLAAN addresses this by reducing early layers’ accuracy to capture more globally useful features, enhancing subsequent layers’ generalization.

Representation Similarity Analysis. To further demonstrate our method’s effectiveness, we conduct Centered Kernel Alignment (CKA) (Kornblith et al. 2019) experiments. We incorporate MLAAN and calculate the CKA (Kornblith et al. 2019) similarity for each layer compared to BP (Rumelhart et al. 1985), then compute the mean values. Results are shown in Figure 6.

MLAAN significantly enhances DGL’s CKA similarity,

particularly in early layers, aligning patterns more closely with BP (Rumelhart et al. 1985). The original method’s poor performance arises from early layers focusing on local optimization, which reduces overall performance.

Conclusion

This paper introduces Multilaminar Leap Augmented Auxiliary Network (MLAAN), a novel approach to resolving issues related to the lack of global features and myopic perspectives that lead to poor performance in existing supervised local learning. MLAAN consists of Multilaminar Local Modules (MLM) and Leap Augmented Modules (LAM). Our MLM addresses the issue of insufficient global features in existing work. We further propose that LAM enhance the auxiliary network for inter-module information exchange, effectively utilizing deeper information to mitigate shortsightedness. We integrate our MLAAN into two SOTA supervised local learning methods and evaluate the performance of different deep network architectures across four widely used datasets. The results demonstrate that our approach significantly enhances the performance of original supervised local learning methods, even surpassing that of E2E training.

References

- Bao, H.; Shu, P.; Zhang, H.; and Liu, X. 2022. Siamese-based twin attention network for visual tracking. *IEEE Transactions on Circuits and Systems for Video Technology*, 33(2): 847–860.
- Bartunov, S.; Santoro, A.; Richards, B.; Marris, L.; Hinton, G. E.; and Lillicrap, T. 2018. Assessing the scalability of biologically-motivated deep learning algorithms and architectures. *Advances in neural information processing systems*, 31.
- Belilovsky, E.; Eickenberg, M.; and Oyallon, E. 2019. Greedy layerwise learning can scale to imagenet. In *International conference on machine learning*, 583–593. PMLR.
- Belilovsky, E.; Eickenberg, M.; and Oyallon, E. 2020. Decoupled greedy learning of cnns. In *International Conference on Machine Learning*, 736–745. PMLR.
- Bengio, Y.; Lamblin, P.; Popovici, D.; and Larochelle, H. 2006. Greedy layer-wise training of deep networks. *Advances in neural information processing systems*, 19.
- Coates, A.; Ng, A.; and Lee, H. 2011. An analysis of single-layer networks in unsupervised feature learning. In *Proceedings of the fourteenth international conference on artificial intelligence and statistics*, 215–223. JMLR Workshop and Conference Proceedings.
- Crick, F. 1989. The recent excitement about neural networks. *Nature*, 337(6203): 129–132.
- DellaFerrera, G.; and Kreiman, G. 2022. Error-driven input modulation: solving the credit assignment problem without a backward pass. In *International Conference on Machine Learning*, 4937–4955. PMLR.
- Deng, J.; Dong, W.; Socher, R.; Li, L.-J.; Li, K.; and Fei-Fei, L. 2009. Imagenet: A large-scale hierarchical image database. In *2009 IEEE conference on computer vision and pattern recognition*, 248–255. Ieee.
- He, K.; Zhang, X.; Ren, S.; and Sun, J. 2016. Deep residual learning for image recognition. In *Proceedings of the IEEE conference on computer vision and pattern recognition*, 770–778.
- He, Y.; Xu, X.; Zhang, J.; Shen, F.; Yang, Y.; and Shen, H. T. 2021. Modeling Two-Stream Correspondence for Visual Sound Separation. *IEEE Transactions on Circuits and Systems for Video Technology*, 32(5): 3291–3302.
- Huo, Z.; Gu, B.; and Huang, H. 2018. Training neural networks using features replay. *Advances in Neural Information Processing Systems*, 31.
- Huo, Z.; Gu, B.; Huang, H.; et al. 2018. Decoupled parallel backpropagation with convergence guarantee. In *International Conference on Machine Learning*, 2098–2106. PMLR.
- Illing, B.; Ventura, J.; Bellec, G.; and Gerstner, W. 2021a. Local plasticity rules can learn deep representations using self-supervised contrastive predictions. *Advances in Neural Information Processing Systems*, 34: 30365–30379.
- Illing, B.; Ventura, J.; Bellec, G.; and Gerstner, W. 2021b. Local plasticity rules can learn deep representations using self-supervised contrastive predictions. *Advances in Neural Information Processing Systems*, 34: 30365–30379.
- Jaderberg, M.; Czarnecki, W. M.; Osindero, S.; Vinyals, O.; Graves, A.; Silver, D.; and Kavukcuoglu, K. 2017a. Decoupled neural interfaces using synthetic gradients. In *International conference on machine learning*, 1627–1635. PMLR.
- Jaderberg, M.; Czarnecki, W. M.; Osindero, S.; Vinyals, O.; Graves, A.; Silver, D.; and Kavukcuoglu, K. 2017b. Decoupled neural interfaces using synthetic gradients. In *International conference on machine learning*, 1627–1635. PMLR.
- Journé, A.; Rodriguez, H. G.; Guo, Q.; and Moraitis, T. 2022. Hebbian deep learning without feedback. *arXiv preprint arXiv:2209.11883*.
- Kornblith, S.; Norouzi, M.; Lee, H.; and Hinton, G. 2019. Similarity of neural network representations revisited. In *International conference on machine learning*, 3519–3529. PMLR.
- Krizhevsky, A.; Hinton, G.; et al. 2009. Learning multiple layers of features from tiny images.
- Le Cun, Y. 1986. Learning process in an asymmetric threshold network. In *Disordered systems and biological organization*, 233–240. Springer.
- Lee, D.-H.; Zhang, S.; Fischer, A.; and Bengio, Y. 2015. Difference target propagation. In *Machine Learning and Knowledge Discovery in Databases: European Conference, ECML PKDD 2015, Porto, Portugal, September 7-11, 2015, Proceedings, Part I 15*, 498–515. Springer.
- Lillicrap, T. P.; Cownden, D.; Tweed, D. B.; and Akerman, C. J. 2014. Random feedback weights support learning in deep neural networks. *arXiv preprint arXiv:1411.0247*.
- Löwe, S.; O’Connor, P.; and Veeling, B. 2019a. Putting an end to end-to-end: Gradient-isolated learning of representations. *Advances in neural information processing systems*, 32.
- Löwe, S.; O’Connor, P.; and Veeling, B. 2019b. Putting an end to end-to-end: Gradient-isolated learning of representations. *Advances in neural information processing systems*, 32.
- Mostafa, H.; Ramesh, V.; and Cauwenberghs, G. 2018. Deep supervised learning using local errors. *Frontiers in neuroscience*, 12: 608.
- Netzer, Y.; Wang, T.; Coates, A.; Bissacco, A.; Wu, B.; and Ng, A. Y. 2011. Reading digits in natural images with unsupervised feature learning.
- Nøkland, A. 2016. Direct feedback alignment provides learning in deep neural networks. *Advances in neural information processing systems*, 29.
- Nøkland, A.; and Eidnes, L. H. 2019. Training neural networks with local error signals. In *International conference on machine learning*, 4839–4850. PMLR.
- Rumelhart, D. E.; Hinton, G. E.; Williams, R. J.; et al. 1985. Learning internal representations by error propagation.
- Salimans, T.; Ho, J.; Chen, X.; Sidor, S.; and Sutskever, I. 2017. Evolution strategies as a scalable alternative to reinforcement learning. *arXiv preprint arXiv:1703.03864*.

- Shen, G.; Zhao, D.; and Zeng, Y. 2022. Backpropagation with biologically plausible spatiotemporal adjustment for training deep spiking neural networks. *Patterns*, 3(6).
- Wang, Y.; Ni, Z.; Song, S.; Yang, L.; and Huang, G. 2021a. Revisiting locally supervised learning: an alternative to end-to-end training. *arXiv preprint arXiv:2101.10832*.
- Wang, Y.; Ni, Z.; Song, S.; Yang, L.; and Huang, G. 2021b. Revisiting locally supervised learning: an alternative to end-to-end training. *arXiv preprint arXiv:2101.10832*.
- Wang, Y.; Peng, C.; and Liu, Y. 2018. Mask-pose cascaded cnn for 2d hand pose estimation from single color image. *IEEE Transactions on Circuits and Systems for Video Technology*, 29(11): 3258–3268.
- Wu, B.; Nair, S.; Martin-Martin, R.; Fei-Fei, L.; and Finn, C. 2021. Greedy hierarchical variational autoencoders for large-scale video prediction. In *Proceedings of the IEEE/CVF Conference on Computer Vision and Pattern Recognition*, 2318–2328.
- Xiong, Y.; Ren, M.; and Urtasun, R. 2020a. Loco: Local contrastive representation learning. *Advances in neural information processing systems*, 33: 11142–11153.
- Xiong, Y.; Ren, M.; and Urtasun, R. 2020b. Loco: Local contrastive representation learning. *Advances in neural information processing systems*, 33: 11142–11153.